Geometry of the octahedral coordination in micas: a review of refined structures

Zdeněk Weiss

Coal Research Institute
71607 Ostrava-Radvanice, Czechoslovakia

Milan Rieder

Institute of Geological Sciences, Charles University
12843 Praha 2, Czechoslovakia

Marta Chmielová and Jan Krajíček

Coal Research Institute
71607 Ostrava-Radvanice, Czechoslovakia

Abstract

Data for 66 refined crystal structures of micas were used to obtain several functions representing the octahedral sheet that served as variables in a statistical analysis: metal–anion bond lengths, two ratios of anion–anion octahedral edges, [1]MEFIR (mean fictive ionic radius), octahedral angle ψ, and counter-rotation of top and bottom anion triads.

All octahedra are flattened, those around larger cations usually more than those around smaller ones. Flattening dominates over counter-rotation in octahedra with large cations and vice versa, as required by the sheet's uniform thickness. Mean counter-rotation in a sheet increases as cation–anion bond lengths are less uniform, suggesting that it results from interactions in the whole sheet. Consequently, both counter-rotation and octahedral angle ψ for individual octahedra can be predicted by regression equations from cation–anion bond lengths or [1]MEFIR for *all* octahedra in the 1M subcell. Thus the octahedral geometry can be checked or predicted from chemistry and an anticipated cation ordering.

Multiple linear regressions yielded a set of cation–anion bond lengths and effective ionic radii for octahedral cations and the vacancy.

Introduction

Since the late twenties and early thirties, when the essential features of the crystal structure of micas were described, the micas continued to receive considerable attention. As the technique of crystal structure analysis improved and as more structures were determined and refined, it became clear that the arrangement of coordination polyhedra is less regular than first thought and that the coordination polyhedra themselves are not ideal. The number of refinements now available provides a sound basis for a synthesis that should give us a better idea about how and why the coordination polyhedra get distorted and how and why they rotate and tilt. Apart from its intrinsic value, such information might be useful to researchers contemplating structural investigations of micas or other layer silicates by permitting them to define their objectives more deliberately or to predict the results more accurately.

We excerpted data from 66 structure refinements published between 1960 and 1984. The set includes 46 trioctahedral and twenty dioctahedral micas of which 51 are natural and fifteen synthetic. Fifty-four structures were refined from X-ray diffraction data, nine from electron and three from neutron diffraction experiments. Most micas belong to the 1M polytype (space group $C2/m$: 37 micas, space group $C2$: four micas), seventeen are $2M_1$, four $2M_2$, and four 3T polytypes. The R factors have a mean at 7.4%, standard deviation of 3.7%, and range from 2.0% to 17.0%. A list of important data for the micas included appears in Table 1.

Treatment of data

Atomic coordinates taken from the original papers were transformed from fractional to absolute and to orthogonal (where non-orthogonal), with the vertical axis parallel to c^*. This included all atoms needed for the construction of complete polyhedra around M1, M2, and M3 cations. (Octahedra with M1 have OH, F, Cl atoms in a *trans*, M2 and M3 in a *cis* arrangement; separate positions M2 and M3 exist in structures without a plane of symmetry, but merge to M2 in others.) Centers of vacancies were defined as lying at one-sixth of the sums of, respectively, the x, y, z coordinates of the six surrounding anions.

There are five functions to which we reduced the geometry of the octahedral sheet: (1) The metal-anion bond lengths $d(M\text{-}A)_{obs}$

Table 1. List of mica structures

No.	Designation	Polytype	R	Type	Method	Material	Reference
1	Dioctahedral mica	1M	10.9	he-di *	E **	M ***	Sidorenko et al. (1975)
2	Dioctahedral Al-mica	1M	16.0	me-di	E	M	Soboleva and Zvyagin (1968)
3	Muscovite	1M	7.0	me-di	E	M	Tsipurskii and Drits (1977)
4	Muscovite	2M$_1$	3.5	me-di	X	M	Güven (1971)
5	Muscovite	2M$_1$	17.0	me-di	X	M	Radoslovich (1960)
6	Muscovite	2M$_1$	12.0	me-di	X	M	Birle and Tettenhorst (1968)
7	Muscovite	2M$_1$	5.0	me-di	E	M	Tsipurskii and Drits (1977)
8	Muscovite	2M$_1$	2.7	me-di	N	M	Rothbauer (1971)
9	Muscovite	2M$_1$	9.9	me-di	X	M	Richardson and Richardson (1982)
10	Dioctahedral mica	2M$_2$	11.7	me-di	E	M	Zhoukhlistov et al. (1973)
11	Muscovite	3T	6.4	he-di	X	M	Güven and Burnham (1967)
12	Phengite	2M$_1$	4.5	me-di	X	M	Güven (1971)
13	Fe-celadonite	1M	10.8	me-di	E	M	Zhukhlistov et al. (1977)
14	Paragonite	1M	12.1	me-di	E	S	Soboleva et al. (1977)
15	Paragonite	2M$_1$	11.1	me-di	E	M	Sidorenko et al. (1977)
16	Paragonite	3T	13.0	he-di	E	M	Sidorenko et al. (1977)
17	Margarite	2M$_1$	16.8	me-di	X	M	Takéuchi (1965)
18	Margarite	2M$_1$	7.5	me-di	X	M	Guggenheim and Bailey (1975)
19	F-polylithionite	1M	5.1	me-tri	X	S	Takeda and Burnham (1969)
20	Lepidolite	1M	6.7	me-tri	X	M	Sartori (1976)
21	Lepidolite	1M	3.5	me-tri	X	M	Guggenheim (1981)
22	Lepidolite	1M	6.2	me-tri	X	M	Guggenheim (1981)
23	Lepidolite	1M	7.3	he-tri	X	M	Backhaus (1983)
24	Lepidolite	2M$_1$	11.3	me-tri	X	M	Sartori (1977)
25	Lepidolite	2M$_1$	9.0	me-tri	X	M	Swanson and Bailey (1981)
26	Lepidolite	2M$_2$	7.2	me-tri	X	M	Takeda et al. (1971)
27	Lepidolite	2M$_2$	10.6	me-tri	X	M	Sartori et al. (1973)
28	Lepidolite	2M$_2$	4.8	me-tri	X	M	Guggenheim (1981)
29	Lepidolite	3T	4.7	he-tri	X	M	Brown (1978)
30	Protolithionite	3T	3.8	he-tri	X	M	Pavlishin et al. (1981)
31	Zinnwaldite	1M	5.7	he-tri	X	M	Guggenheim and Bailey (1977)
32	Phlogopite	1M	4.1	ho-tri	X	M	Hazen and Burnham (1973)
33	Phlogopite	1M	13.1	ho-tri	X	M	Steinfink (1962)
34	Phlogopite	1M	5.0	ho-tri	N	M	Rayner (1974)
35	Phlogopite	1M	2.0	ho-tri	N	M	Joswig (1972)
36	Mg-mica	1M	2.9	ho-tri	X	S	Toraya et al. (1978)
37	Tetraferriphlogopite	1M	4.2	ho-tri	X	M	Semenova et al. (1977)
38	F-phlogopite	1M	6.1	ho-tri	X	S	McCauley et al. (1973)
39	Li,F-phlogopite	1M	7.3	ho-tri	X	S	Takeda and Donnay (1966)
40	Mn,Ba-phlogopite	1M	8.1	ho-tri	X	M	Kato et al. (1979)
41	Mn,Ba-phlogopite	1M	10.6	ho-tri	X	M	Kato et al. (1979)
42	Mn,Ba-phlogopite	1M	6.0	ho-tri	X	M	Kato et al. (1979)
43	Kinoshitalite	1M	7.8	ho-tri	X	M	Kato et al. (1979)
44	F-mica	1M	3.8	ho-tri	X	S	Toraya et al. (1976)
45	Trioctahedral mica	1M	3.0	ho-tri	X	M	Hazen and Burnham (1981)
46	Biotite	1M	4.4	me-tri	X	M	Takeda and Ross (1975)
47	Biotite	2M$_1$	5.6	me-tri	X	M	Takeda and Ross (1975)
48	Mn-biotite	1M	12.1	me-tri	X	M	Kato et al. (1979)
49	Oxybiotite	1M	4.4	me-tri	X	M	Ohta et al. (1982)
50	Oxybiotite	2M$_1$	3.9	me-tri	X	M	Ohta et al. (1982)
51	Annite	1M	4.4	me-tri	X	M	Hazen and Burnham (1973)
52	Trioctahedral Fe-mica	1M	9.3	ho-tri	X	S	Donnay et al. (1964)
53	Taeniolite	1M	2.4	me-tri	X	S	Toraya et al. (1977)
54	Mg-mica	1M	9.2	me-tri	X	S	Tateyama et al. (1974)
55	Ge-mica	1M	3.8	me-tri	X	S	Toraya et al. (1978)
56	Ge-mica	1M	5.5	me-tri	X	S	Toraya et al. (1978)
57	Ge-mica	1M	3.7	ho-tri	X	S	Toraya et al. (1978)
58	Xanthophyllite	1M	10.8	me-tri	X	M	Takéuchi (1965)
59	Bityite	2M$_1$	11.5	me-tri	X	M	Sokolova et al. (1979)
60	Ephesite	1M	11.5	me-tri	X	M	Sokolova et al. (1979)
61	Ba-mica	1M	7.1	ho-tri	X	S	McCauley and Newnham (1973)
62	Hendricksite	1M	7.2	ho-tri	X	M	Robert and Gasperin (1984)
63	Chernykhite	2M$_1$	12.0	me-di	X	M	Rozhdestvenskaya and Frank-Kamenetskii (1974)
64	Mn,F-mica	1M	4.3	ho-tri	X	S	Toraya et al. (1983)
65	Ge-mica	1M	4.2	me-tri	X	S	Toraya and Marumo (1983)
66	Paragonite	2M$_1$	4.5	me-di	X	M	Lin and Bailey (1984)

 * di = dioctahedral, tri = trioctahedral, ho = homooctahedral, me = mesooctahedral, he = heterooctahedral

 ** X = X-ray diffraction, E = electron diffraction, N = neutron diffraction

*** M = mineral, S = synthetic

Except for 'Type', all information is taken over from the original papers.

given in the original papers were checked and supplemented with those for vacancy-anion in structures containing vacant sites. (2) The lengths of anion-anion edges, checked and corrected, were used to compute ratios R_1 = *mean unshared edge/mean shared edge* (Toraya, 1981) and R_2 = *mean of longer shared edges/mean of shorter shared edges*. (3) The ^{1}MEFIR, *mean fictive ionic radius* of Hoppe (1979) was calculated for each cation from *fictive ionic radii* (FIR), which are defined as bond lengths divided in proportion to the radii of cation (r_M) and anion (r_A):

$$\text{FIR}_j = d(M - A)_{\text{obs } j} \cdot r_M/(r_M + r_{Aj}).$$

The ^{1}MEFIR$_{\text{obs}}$ is a weighted mean of FIR$_j$:

$$^1\text{MEFIR}_{\text{obs}} = \sum_{j=1}^{j=6} w_j \cdot \text{FIR}_j \Big/ \sum_{j=1}^{j=6} w_j$$

where $w_j = \exp[1 - (\text{FIR}_j/\text{FIR}_{\text{min}})^6]$, FIR$_{\text{min}}$ being the smallest FIR$_j$ in an octahedron. Hoppe's (1979) formula is a sum from one to infinity, but we limited the summation to the six nearest neighbors because the second coordination sphere did not affect the values obtained. (4) The octahedral angle ψ and (5) the counter-rotation δ are defined and illustrated in Figure 1 (note that δ is not identical with ω of Appelo, 1978). The thickness of the octahedral sheet t_{oct}, which is used to compute ψ, is the difference between mean vertical coordinates for, respectively, the top and bottom anion triads in an octahedron. These data appear in Table 2.

Among the above functions, R_1 and R_2 are easier to calculate than ψ and δ. Fortunately, there is an excellent relation between ψ and R_1 permitting an easy conversion ($\psi = 37.96 R_1 + 16.95$, correlation coefficient $r = 0.999$, number of data $n = 198$). Practically the same holds for δ and R_2 (Fig. 2), where two relations appear, one for larger and one for smaller cations (there is one larger cation per two smaller in muscovite-type structures, the inverse holds for xanthophyllite-type). Data for homooctahedral micas, which are a trivial case common to both series, cluster near the origin, but yield a good regression relation. The δ values required can be obtained from R_2 by means of appropriate equations in Figure 2. For the sake of lucidity we preferred ψ and δ throughout this paper.

Multiple linear regressions of bond lengths and ^{1}MEFIR are based on equations of the type

$$d(M - O)_{\text{obs}} = \sum_i d(M - O)_i \cdot X_i$$

where the atomic fractions X_i ε $< 0.0; 1.0 >$ and $\sum_i X_i = 1.0$. Bond lengths metal–oxygen $d(M-O)_i$ or ^{1}MEFIR$_i$ obtained by regression will be referred to as *partial*, to differentiate them from experimental ones for octahedra occupied by one cation only. This
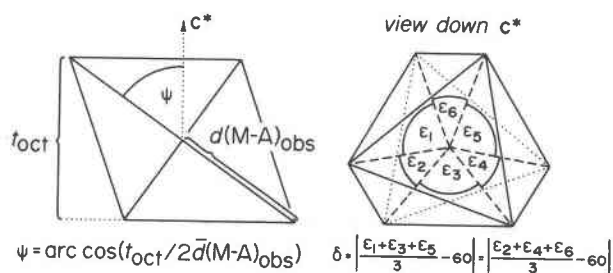
is because these quantities are equal to *partial derivatives* of $d(M-O)_{\text{obs}}$ with respect to atomic fractions X_i. Correlation coefficients were computed as

$$r^2 = 1.0 - \sum_i (y_i - y_{\text{calc}})^2 \Big/ \sum_i (y_i - \bar{y})^2.$$

Several computer programs were written and used to perform these and other calculations.

Results

Regression analysis of bond lengths and ^{1}MEFIR

These results are in fact by-products. In order to be able to calculate ^{1}MEFIR$_{\text{obs}}$ for individual octahedra, we needed a radius of the vacancy. The most straightforward way was to subtract 1.26Å (crystal radius of oxygen in coordination VI, Shannon, 1976) from the partial vacancy-oxygen "bond length" obtained by multiple linear regression of bond lengths, $d(M-O)_{\text{obs}}$. The resulting radius of 0.97Å was combined with the crystal radii of Shannon (1976) to yield FIR$_j$ and ^{1}MEFIR$_{\text{obs}}$ reflecting proportions of cations on individual sites. The ^{1}MEFIR$_{\text{obs}}$ thus obtained, in turn, were subjected to multiple linear regression yielding a set of partial ^{1}MEFIR$_i$.

Our partial bond lengths (Table 3) compare fairly well to bond lengths of Drits (1975) based on various layer silicates (correlation coefficient 0.91). There is also a good agreement between partial ^{1}MEFIR$_i$ and the crystal radii of Shannon (1976) (correlation coefficient 0.95, Na$^+$, Ca^{2+}, V^{3+} and V^{4+} not included).

A few points merit mentioning. First, the partial "bond length" for vacancy-oxygen and the partial ^{1}MEFIR$_i$ for vacancy calculate with small errors. True, the vacancy is among the most frequent "cations", which increases the precision; but the main cause must be the tendency of the octahedral sheet to impose a constant size on vacant sites. By the same token, the presently obtained 0.96Å applies to the octahedral sheet of micas, but not necessarily even to the same coordination in different structures (Barry and Roy, 1967). Second, Table 3 has entries for Na$^+$, Ca^{2+}, Zn^{2+}, V^{3+} and V^{4+}, which were reported in only a few octahedra. The partial ^{1}MEFIR$_i$ for Na$^+$ and Ca^{2+}, although exhibiting the biggest difference from Shannon's radii, is the largest of all and cannot be confused; thus the presence of Na$^+$ and Ca^{2+} in octahedral sheets must be real. Third, the bond lengths are a product of crystal structure refinements only, but the ^{1}MEFIR$_{\text{obs}}$ are calculated from bond lengths *and* input radii. As a check of consistency, we calculated apparent ionic radii of oxygen by subtracting partial ^{1}MEFIR$_i$ from the corresponding partial $d(M-O)_i$. A weighted mean with weights proportional to the reciprocals of estimated variances equals 1.25Å, which is acceptably close to the 1.26Å (Shannon, 1976) used at the outset. Consequently, the ^{1}MEFIR$_{\text{obs}}$ and the partial ^{1}MEFIR$_i$ are directly comparable to ionic radii.

Distortions of octahedra

The relationships obtained in the present review did not warrant a separate treatment of dioctahedral and triocta-

Fig. 1. Octahedral angle ψ and counter-rotation δ represent distortions of the octahedral sheet. Angles ε_i are measured in projection onto the **ab** plane, $\bar{d}(M-A)_{\text{obs}}$ is the mean cation–anion bond length in an octahedron.

$\psi = \text{arc} \cos(t_{\text{oct}}/2\bar{d}(M-A)_{\text{obs}})$

$\delta = \left| \frac{\varepsilon_1 + \varepsilon_3 + \varepsilon_5}{3} - 60 \right| = \left| \frac{\varepsilon_2 + \varepsilon_4 + \varepsilon_6}{3} - 60 \right|$

Table 2. Data for individual octahedra

No.	$\bar{d}(M-A)_{obs}$	ψ	δ	$^1MEFIR_{obs}$	$\bar{d}(A-A)_{obs}$	R_1	R_2	t_{oct}*
1 M1	2.220	61.6	1.44	0.968	3.130	1.175	1.020	2.114
M2	1.921	56.6	13.18	0.673	2.718	1.044	1.154	
M3	1.958	57.3	14.57	0.700	2.770	1.061	1.177	
2 M1	2.153	59.4	0.00	0.938	3.042	1.117	1.000	2.192
M2	1.993	56.6	7.80	0.693	2.819	1.045	1.089	
3 M1	2.262	61.5	0.00	0.988	3.189	1.174	1.000	2.158
M2	1.947	56.3	15.67	0.700	2.757	1.037	1.183	
4 M1	2.245	62.1	0.00	0.979	3.164	1.188	1.000	2.104
M2	1.932	57.0	15.45	0.683	2.736	1.054	1.186	
5 M1	2.204	61.2	0.00	0.950	3.108	1.165	1.000	2.121
M2	1.955	57.1	12.13	0.689	2.767	1.056	1.143	
6 M1	2.258	62.3	0.00	0.986	3.180	1.195	1.000	2.097
M2	1.925	57.0	16.63	0.679	2.725	1.052	1.201	
7 M1	2.247	62.2	0.00	0.981	3.166	1.193	1.000	2.094
M2	1.927	57.1	15.86	0.682	2.728	1.055	1.192	
8 M1	2.241	62.2	0.00	0.978	3.159	1.193	1.000	2.089
M2	1.930	57.2	15.35	0.680	2.732	1.059	1.187	
9 M1	2.253	61.9	0.00	0.983	3.176	1.184	1.000	2.124
M2	1.940	56.8	15.40	0.686	2.747	1.050	1.185	
10 M1	2.195	60.9	0.00	0.956	3.096	1.158	1.000	2.134
M2	1.956	56.9	11.80	0.689	2.767	1.052	1.138	
11 M1	2.231	61.7	2.35	0.968	3.147	1.178	1.034	2.113
M2	1.913	56.5	13.06	0.671	2.707	1.040	1.151	
M3	1.971	57.6	15.35	0.703	2.793	1.068	1.189	
12 M1	2.223	61.4	0.00	0.970	3.134	1.171	1.000	2.127
M2	1.956	57.1	12.92	0.717	2.768	1.056	1.155	
13 M1	2.141	58.3	0.00	0.935	3.025	1.090	1.000	2.249
M2	2.045	56.6	4.60	0.757	2.888	1.046	1.052	
14 M1	2.091	59.9	0.00	0.913	2.952	1.130	1.000	2.100
M2	1.970	57.8	5.78	0.698	2.784	1.076	1.069	
15 M1	2.160	60.5	0.00	0.941	3.049	1.148	1.000	2.125
M2	1.950	57.0	10.27	0.690	2.758	1.054	1.121	
16 M1	2.061	59.7	0.67	0.851	2.909	1.128	1.008	2.076
M2	1.965	58.0	3.76	0.708	2.777	1.085	1.046	
M3	1.981	58.4	4.41	0.732	2.799	1.092	1.055	
17 M1	2.203	61.9	0.00	0.960	3.105	1.184	1.000	2.076
M2	1.912	57.1	14.51	0.670	2.707	1.057	1.174	
18 M1	2.193	61.8	0.43	0.956	3.091	1.181	1.006	2.074
M2	1.902	57.0	14.19	0.666	2.690	1.052	1.169	
19 M1	2.106	60.2	0.00	0.851	2.972	1.138	1.000	2.096
M2	1.981	58.1	5.86	0.761	2.799	1.083	1.071	
20 M1	2.113	60.8	0.00	0.882	2.981	1.155	1.000	2.060
M2	1.972	58.5	6.56	0.747	2.786	1.095	1.082	
21 M1	2.118	60.9	0.00	0.889	2.988	1.159	1.000	2.057
M2	1.970	58.5	6.88	0.748	2.784	1.096	1.087	
22 M1	2.119	60.4	10.09	0.874	2.991	1.143	1.142	2.093
M2	1.878	56.2	0.27	0.685	2.657	1.036	1.003	
23 M1	2.098	60.5	0.00	0.865	2.961	1.147	1.082	2.066
M2	1.913	57.3	1.97	0.671	2.704	1.065	1.023	
M3	2.058	59.9	7.98	0.840	2.906	1.129	1.108	
24 M1	2.121	60.9	0.00	0.894	2.992	1.156	1.000	2.062
M2	1.976	58.6	6.66	0.751	2.792	1.094	1.083	
25 M1	2.107	60.7	0.00	0.882	2.972	1.153	1.000	2.062
M2	1.977	58.6	6.00	0.759	2.793	1.096	1.075	
26 M1	2.144	61.0	0.00	0.910	3.024	1.161	1.000	2.077
M2	1.967	58.1	8.32	0.742	2.780	1.084	1.104	
27 M1	2.123	60.8	0.00	0.887	2.996	1.154	1.000	2.074
M2	1.980	58.4	6.66	0.750	2.798	1.092	1.083	
28 M1	2.121	61.1	0.00	0.893	2.992	1.162	1.000	2.053
M2	1.966	58.5	7.22	0.750	2.780	1.096	1.091	
29 M1	2.036	59.6	8.20	0.766	2.868	1.117	1.110	2.060
M2	1.920	57.6	4.10	0.677	2.716	1.068	1.046	
M3	2.113	60.8	4.40	0.882	2.980	1.153	1.061	
30 M1	2.120	60.4	9.90	0.839	2.994	1.145	1.139	2.092
M2	1.908	56.8	1.40	0.671	2.699	1.051	1.016	
M3	2.149	60.9	8.50	0.850	3.032	1.156	1.121	
31 M1	2.132	60.8	10.10	0.851	3.014	1.156	1.145	2.079
M2	1.882	56.5	0.06	0.663	2.666	1.044	1.001	
M3	2.131	60.8	10.10	0.849	3.012	1.155	1.146	
32 M1	2.063	59.0	0.00	0.843	2.914	1.108	1.000	2.126
M2	2.064	59.0	0.05	0.843	2.916	1.109	1.001	
33 M1	2.101	58.1	0.00	0.856	2.969	1.086	1.000	2.219
M2	2.105	58.2	0.16	0.857	2.975	1.087	1.002	
34 M1	2.077	59.2	0.00	0.845	2.932	1.113	1.000	2.127
M2	2.064	59.0	0.54	0.840	2.915	1.107	1.007	
35 M1	2.066	59.2	0.00	0.838	2.919	1.113	1.000	2.117
M2	2.063	59.1	0.18	0.837	2.913	1.111	1.003	
36 M1	2.062	58.8	0.00	0.845	2.913	1.103	1.000	2.138
M2	2.063	58.8	0.04	0.846	2.914	1.103	1.001	
37 M1	2.085	59.0	0.00	0.846	2.945	1.109	1.000	2.147
M2	2.085	59.0	0.02	0.847	2.945	1.109	1.001	
38 M1	2.062	59.0	0.00	0.846	2.912	1.108	1.000	2.124
M2	2.065	59.0	0.12	0.847	2.916	1.109	1.002	
39 M1	2.061	59.3	0.00	0.847	2.911	1.117	1.000	2.102
M2	2.060	59.3	0.07	0.846	2.909	1.116	1.001	
40 M1	2.122	57.9	0.00	0.853	3.000	1.080	1.000	2.255
M2	2.113	57.8	0.41	0.849	2.987	1.076	1.005	
41 M1	2.101	58.4	0.00	0.845	2.968	1.092	1.000	2.203
M2	2.090	58.2	0.43	0.841	2.955	1.087	1.005	
42 M1	2.087	58.8	0.00	0.829	2.947	1.102	1.000	2.163
M2	2.079	58.7	0.34	0.827	2.936	1.099	1.004	
43 M1	2.095	58.6	0.00	0.837	2.961	1.097	1.000	2.185
M2	2.087	58.4	0.40	0.833	2.949	1.093	1.005	
44 M1	2.062	58.0	0.00	0.855	2.915	1.082	1.000	2.187
M2	2.064	58.0	0.06	0.856	2.917	1.083	1.000	
45 M1	2.077	58.8	0.00	0.858	2.934	1.103	1.000	2.152
M2	2.077	58.8	0.02	0.858	2.934	1.103	1.000	
46 M1	2.086	58.9	0.00	0.815	2.946	1.112	1.000	2.139
M2	2.068	58.9	0.76	0.807	2.921	1.104	1.009	
47 M1	2.086	59.2	0.00	0.815	2.947	1.111	1.000	2.136
M2	2.067	58.9	0.78	0.801	2.922	1.104	1.010	
48 M1	2.120	57.5	0.00	0.810	3.004	1.072	1.000	2.278
M2	2.130	57.7	0.16	0.813	3.010	1.073	1.002	
49 M1	2.077	59.4	0.00	0.802	2.933	1.120	1.000	2.112
M2	2.059	59.1	0.83	0.782	2.906	1.111	1.010	
50 M1	2.076	59.4	0.00	0.801	2.932	1.119	1.000	2.114
M2	2.060	59.1	0.74	0.784	2.907	1.111	1.009	
51 M1	2.121	58.6	0.00	0.809	2.996	1.098	1.000	2.208
M2	2.101	58.3	0.87	0.801	2.968	1.090	1.011	
52 M1	2.107	59.3	0.00	0.790	2.973	1.117	1.000	2.153
M2	2.107	59.3	0.03	0.790	2.972	1.116	1.000	
53 M1	2.058	57.8	0.00	0.851	2.909	1.078	1.000	2.193
M2	2.061	57.9	0.13	0.853	2.913	1.079	1.000	
54 M1	2.083	58.0	0.00	0.851	2.943	1.084	1.000	2.206
M2	2.094	58.2	0.50	0.859	2.959	1.088	1.006	
55 M1	2.092	59.3	0.00	0.867	2.955	1.115	1.000	2.139
M2	2.092	59.3	0.03	0.866	2.955	1.115	1.000	
56 M1	2.179	60.1	0.00	0.919	3.074	1.137	1.000	2.171
M2	2.070	58.9	4.79	0.852	2.925	1.092	1.059	
57 M1	2.076	60.2	0.00	0.846	2.929	1.140	1.000	2.064
M2	2.078	60.2	0.09	0.847	2.933	1.140	1.002	
58 M1	2.019	57.8	0.00	0.768	2.853	1.078	1.000	2.150
M2	2.072	58.7	1.42	0.838	2.906	1.098	1.017	
59 M1	2.178	61.7	0.15	0.890	3.065	1.181	1.002	2.067
M2	1.891	56.9	13.85	0.606	2.683	1.058	1.166	
60 M1	2.130	61.3	0.05	0.898	3.004	1.166	1.001	2.047
M2	1.920	57.8	9.98	0.674	2.725	1.076	1.120	
61 M1	2.073	58.7	0.00	0.856	2.929	1.100	1.000	2.156
M2	2.062	58.5	0.50	0.852	2.913	1.095	1.006	
62 M1	2.093	58.5	0.00	0.843	2.957	1.095	1.000	2.188
M2	2.088	58.4	0.20	0.842	2.952	1.092	1.000	
63 M1	2.244	60.4	0.00	0.967	3.166	1.144	1.000	2.217
M2	2.013	56.6	10.96	0.751	2.849	1.044	1.127	
64 M1	2.071	58.4	0.00	0.854	2.926	1.092	1.000	2.172
M2	2.071	58.4	0.00	0.854	2.926	1.092	1.000	
65 M1	2.103	59.6	0.00	0.867	2.969	1.123	1.000	2.130
M2	2.091	59.4	0.50	0.858	2.953	1.118	1.006	
66 M1	2.221	62.1	0.00	0.969	3.130	1.190	1.000	2.077
M2	1.908	57.0	15.70	0.670	2.701	1.054	1.190	

* octahedral thickness

hedral micas, so this traditional division was abandoned in favor of a more expedient one based on the symmetry of occupancy of individual octahedral sites: in *homooctahedral* micas crystallochemical entities (cations) in all three octahedra are identical; two are identical and one different in *mesooctahedral*; and all are different in *heterooctahedral*[1]. We considered two octahedra as identical if the cations inside them are chemically identical (or, if the chemical identity is not stated explicitly, if they have the same scattering power) *and* if their mean metal–anion bond lengths differ by ≤ 1 *esd* given by the authors of the structure refinement. Our set contains 7 heterooctahedral, 39 mesooctahedral, and 20 homooctahedral micas.

As a reconnaissance, we examined the relations between ψ, δ, and $^1MEFIR_{obs}$. A plot of ψ vs. $^1MEFIR_{obs}$ (Fig. 3) is quite interesting. First, not a single octahedron is ideal, the closest to ideality being flattened by about $1\frac{1}{2}°$ (all occupied

[1] These terms are introduced for purposes of this paper and are not meant for general use unless approved by the I.M.A.

Fig. 2. Relations between ratio R_2 (*mean of longer shared edges/ mean of shorter shared edges*) and counter-rotation δ, permitting an estimation of δ from R_2. For more clarity, homooctahedral micas are not plotted; however, the corresponding regression equation is included.

with Al). There is no self-apparent reason why octahedra combined in a sheet should be geometrically ideal, but it is interesting to note that a regression line through all data points reaches the ideal geometry for $^1MEFIR_{obs} \approx 0.52Å$. Second, the plot suffers from more scatter than one would expect from such precise data. It does not diminish if just structures with a small R factor are plotted or if we plot only data for octahedra lying on a plane of symmetry ($\delta = 0°$, all open and most solid circles in Fig. 3). Hence the

scatter is not a matter of the precision of refinement nor is it associated with the magnitude of counter-rotation δ. Third, and most interesting, there is an overall tendency for larger cations to occupy more flattened octahedra. In fact, there might be one relationship for cis octahedra and another, moderately different, for trans (see regression lines in Fig. 3).

The last point is at variance with the conclusion of Hazen and Wones (1972, Fig. 7) based on micas with octahedral sheets fully occupied with Fe^{2+}, Co^{2+}, Cu^{2+}, Mg^{2+}, and Ni^{2+}, respectively. Hazen and Wones (1972) used the formula derived by Donnay et al. (1964)

$$\sin \psi = \frac{b}{3\sqrt{3}\,\bar{d}(M-A)},$$

obviously unsuitable for micas with different cations in different octahedra whose contributions to the b parameter tend to cancel each other. Although more general, our formula (used e.g. by Guggenheim and Bailey, 1977) must give practically the same results as that of Hazen and Wones for their micas. This is seen on homooctahedral micas in Figure 3, which outline a poorly correlated trend similar to that of Hazen and Wones (1972). The only safe conclusion that can be drawn from Figure 3 is that the octahedral angle ψ is not a simple function of the size of the cation inside an octahedron (see also Lin and Guggenheim, 1983).

A plot of counter-rotation δ vs. $^1MEFIR_{obs}$ indicates no meaningful relationship at all. There is very little improvement even if octahedra with $\delta = 0°$ (lying on a plane of symmetry) are left out. More strikingly than ψ, δ of an octahedron is in no simple relation to the size of its occupant.

Both distortion functions could still be related to each

Table 3. Partial bond lengths and partial ^1MEFIR for octahedral cations in micas, and distribution of cations between larger and smaller octahedra

	m *	$d(M-O)_1$ present work	$d(M-O)$ Drits (1975)	$^1MEFIR_1$ present work	Crystal radii ^{VI} Shannon (1976)	Mean composition of cations in octahedra ** larger	smaller
Al^{3+}	105	1.914(4) Å	1.922 Å	0.671(2) Å	0.675 Å	0.033	0.627
Fe^{2+}	56	2.113(11)	2.120	0.792(4)	0.75 ***	0.066	0.044
Mg^{2+}	123	2.085(4)	2.075	0.847(2)	0.86	0.190	0.159
Li^+	55	2.116(8)	2.160	0.885(3)	0.90	0.266	0.080
Mn^{2+}	38	2.194(24)		0.843(9)	0.81	0.008	0.002
Fe^{3+}	46	2.057(27)	1.990	0.724(11)	0.69 ***	0.013	0.036
Ti^{4+}	29	2.271(68)		0.715(27)	0.745	0.005	0.014
Na^+ , Ca^{2+}	7	2.424(243)		0.916(95)	1.16 , 1.14	0.002	0.000
Zn^{2+}	3	2.033(89)		0.874(35)	0.88	0.000	0.000
V^{3+} , V^{4+}	2	2.025(24)		0.772(9)	0.78 , 0.72	0.000	0.019
vacancy	79	2.233(6)		0.963(2)		0.417	0.019
n	396			198		53	85
r	0.924			0.993			

* number of octahedra containing the cation

** ordered structures only (homooctahedral micas not included)

*** low spin
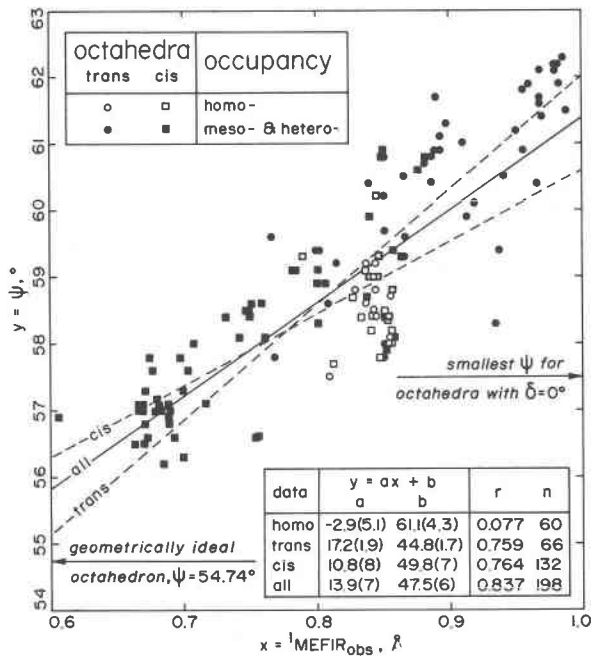
Fig. 3. Relation between $^1\text{MEFIR}_{\text{obs}}$ (cation radius) and octahedral angle ψ. Angle ψ for a geometrically ideal octahedron would be realized for $^1\text{MEFIR}_{\text{obs}} \approx 0.52\text{Å}$.

other. To test if they are, we transformed ψ and δ values to dimensionless and mutually comparable ψ_{tr} and δ_{tr} by subtracting the respective means and dividing by corresponding standard deviations. When plotted against $^1\text{MEFIR}_{\text{obs}}$,
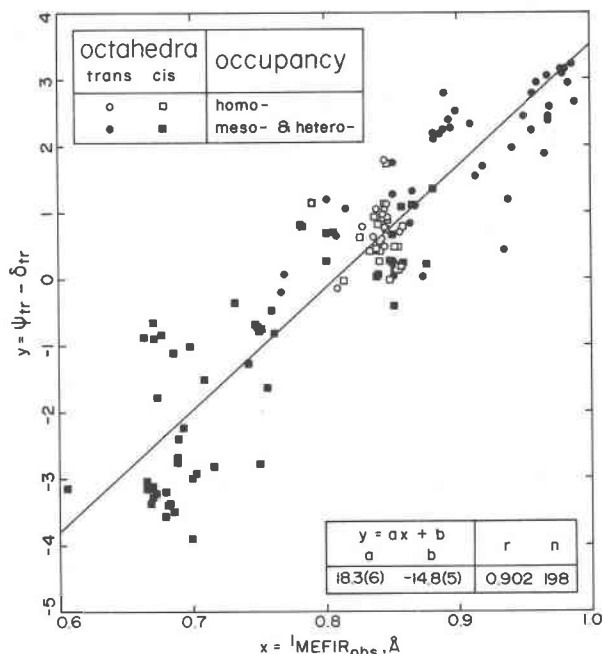
Fig. 4. The difference between transformed octahedral angle ψ_{tr} and counter-rotation δ_{tr} plotted as a function of $^1\text{MEFIR}_{\text{obs}}$.
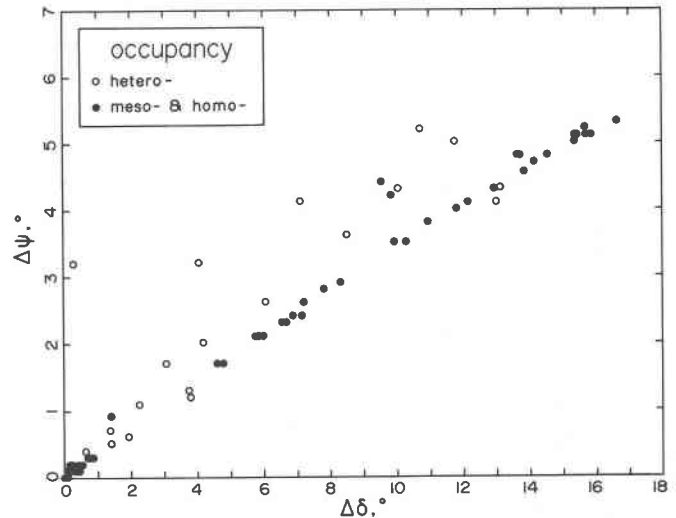
Fig. 5. Differences of ψ in a sheet, that is $|\psi(\text{M1}) - \psi(\text{M2})|$, $|\psi(\text{M2}) - \psi(\text{M3})|$, $|\psi(\text{M3}) - \psi(\text{M1})|$, plotted against corresponding differences of δ. Inasmuch as both variables are a function of a common cause rather than of one another, no lines were fitted through the data points. A total of 198 points is shown, 59 of which plot at the origin.

the sum $\psi_{\text{tr}} + \delta_{\text{tr}}$ shows no functional dependence. The points concentrate about $\psi_{\text{tr}} + \delta_{\text{tr}} = 0$ and spread parallel to the $^1\text{MEFIR}_{\text{obs}}$ axis. Even though there is considerable scatter, the pattern is that corresponding to a case where ψ_{tr} and δ_{tr} in an octahedron *compensate* each other. Therefore, we plotted $\psi_{\text{tr}} - \delta_{\text{tr}}$ vs. $^1\text{MEFIR}_{\text{obs}}$ (Fig. 4). The result is a fairly tight positively sloping linear relation. Inasmuch as positive values of ψ_{tr} and δ_{tr} correspond to larger-than-average octahedral angles (flatter octahedra) or counter-rotations, respectively, positive $\psi_{\text{tr}} - \delta_{\text{tr}}$ represents octahedra with more flattening than counter-rotation, while negative $\psi_{\text{tr}} - \delta_{\text{tr}}$ marks more upright octahedra with considerable counter-rotation. Puzzling at first sight, the result is a predictable consequence of the octahedral sheet's uniform thickness.

An important hint comes from the plot of $\Delta\delta$ vs. $\Delta\psi$ (Fig. 5). Despite some recalcitrant points belonging to heterooctahedral micas, the plot shows an impressive correlation between the differences of δ and ψ in the octahedral sheet. It supports the conclusion anticipated when interpreting relations between ψ, δ, and $^1\text{MEFIR}_{\text{obs}}$: both distortions in a particular octahedron are due to interaction in the whole sheet rather than the octahedron alone (analogous conclusions were drawn from 26 refinements by Lin and Guggenheim, 1983, who approached the problem from a different angle). Consequently, to unravel the causes of distortions, variables representing the whole sheet have to be employed.

One such variable is a measure of scatter (we opted for the *esd* divided by the mean), the mean is another. In Figures 6 and 7 the abscissae represent the scatter of bond lengths $d(\text{M-A})_{\text{obs}}$ and the scatter of $^1\text{MEFIR}_{\text{obs}}$ in individ-
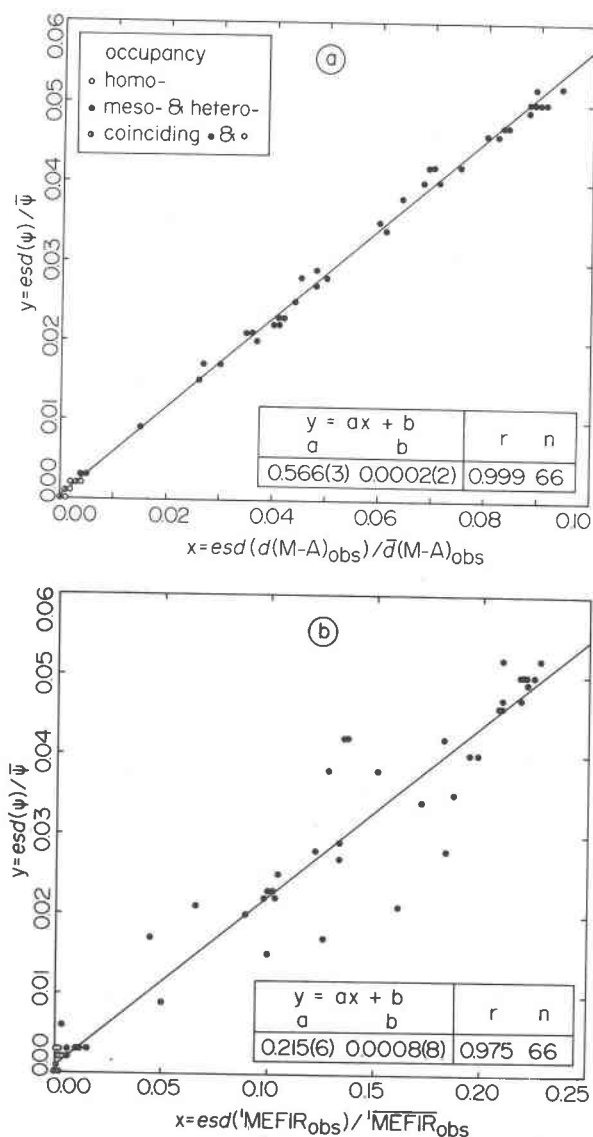
Fig. 6. Measure of scatter of ψ angle in a sheet, $esd(\psi)/\bar{\psi}$, plotted against the same function of bond length $d(M\text{-}A)_{obs}$ (a) and $^1MEFIR_{obs}$ (b).

that $^1MEFIR_{obs}$, a mere scalar, implies a spherical entity, while the bond lengths allow for the more realistic anisotropism. Second, Figure 7a indicates that once there is an ordering among the octahedral cations, bond lengths are its direct consequence and they, in turn, determine the counter-rotation δ. A different form of the same was observed by Lin and Guggenheim (1983) who correlated counter-rotation ω (Appelo, 1978) with the ratio $\bar{d}(M1\text{-}A)/\bar{d}(M2\text{-}A)$. Finally, the fact that correlations between pairs of independent variables as good as those in Figures 6a and 7a can be obtained signifies that the octahedral sheet cannot be under much stress from both the interlayer and the tetrahedral sheet. In other words, the octahedral sheet must be the most rigid element in the
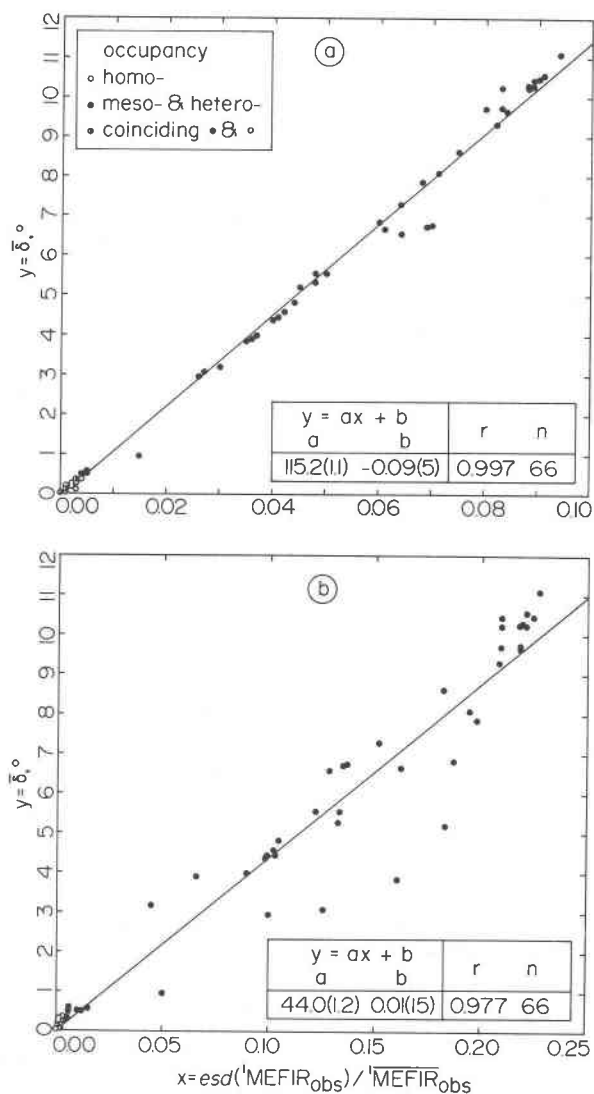
Fig. 7. Mean counter-rotation $\bar{\delta}$ in a sheet plotted against the measure of scatter (esd/mean) of bond lengths $d(M\text{-}A)_{obs}$ (a) and $^1MEFIR_{obs}$ (b).

ual octahedral sheets. Along the ordinate is plotted the scatter of ψ (Fig. 6) and $\bar{\delta}$ (Fig. 7). Inasmuch as uniformity of bond lengths or $^1MEFIR_{obs}$ (no scatter) signifies a $\bar{\delta} = 0°$, Figure 7 yields a nonzero $\bar{\delta}$ if there is scatter; $\bar{\delta}$, in turn, is easily converted to δ for individual octahedra in homooctahedral and mesooctahedral micas. However, uniformity of bond lengths or $^1MEFIR_{obs}$ does not spell an unequivocal $\bar{\psi}$ and therefore the plot in Figure 6 is as far as we can go without introducing another variable.

Several valuable general conclusions can be drawn from Figures 6 and 7. First, the correlations including scatter of $d(M\text{-}A)_{obs}$ are considerably better behaved than those including scatter of $^1MEFIR_{obs}$. This has to do with the fact

Table 4. Constants in regression equations for predicting octahedral angle ψ from mean bond lengths $\bar{d}(M\text{-}A)_{obs}$ and $^1MEFIR_{obs}$.*

		Micas (n)					
		Heterooctahedral (7) **		Mesooctahedral (39)		Homooctahedral (20) **	
		Regression based on		Regression based on		Regression based on	
Equation for		$^1MEFIR_{obs}$	$\bar{d}(M\text{-}A)_{obs}$	$^1MEFIR_{obs}$	$\bar{d}(M\text{-}A)_{obs}$	$^1MEFIR_{obs}$	$\bar{d}(M\text{-}A)_{obs}$
ψ(M1)	a_1	4.8	8.1	8.6	8.3	-2.7	-15.8
	a_2	-35.7	-11.8	-10.2	-11.9	***	***
	a_3	-4.8	-2.9	***	***	***	***
	a_4	84.3	71.8	60.3	66.2	60.9	91.5
	r	0.998	0.998	0.844	0.916	0.078	0.519
ψ(M2)	a_1	1.7	-7.5	-7.3	-7.4	***	
	a_2	44.7	6.2	5.9	5.1		
	a_3	5.5	-2.7	***	***		
	a_4	21.0	66.8	60.0	63.4		
	r	0.943	0.996	0.828	0.793		
ψ(M3)	a_1	0.3	-7.7	***		***	
	a_2	4.0	-11.9				
	a_3	20.2	13.4				
	a_4	40.3	71.2				
	r	0.979	0.999				

* $\psi(M1, M2, M3) = a_1 \, ^1MEFIR_{obs}(M1) + a_2 \, ^1MEFIR_{obs}(M2) + a_3 \, ^1MEFIR_{obs}(M3) + a_4$

   $\psi(M1, M2, M3) = a_1 \, \bar{d}(M1\text{-}A)_{obs} + a_2 \, \bar{d}(M2\text{-}A)_{obs} + a_3 \, \bar{d}(M3\text{-}A)_{obs} + a_4$

** Some of the errors (not shown) exceed the associated constants, apparently due to paucity of data.

*** M3 is not defined in homooctahedral and mesooctahedral micas, and M2 is geometrically identical with M1 in homooctahedral micas.

structure of micas, subject to only subordinate influence from the rest of the structure (see also Radoslovich and Norrish, 1962).

Spurred by the preceding, we performed a final set of calculations to obtain regression equations suitable for predicting octahedral angle ψ and counter-rotation δ in octahedra M1, M2, and M3 (where defined) from either bond lengths or $^1MEFIR_{obs}$ (or cation radii) for *all* octahedra in a sheet. The size constraints inherent in the definition of mesooctahedral and homooctahedral micas dictate the number of constants necessary: it is highest in heterooctahedral micas and lowest in homooctahedral. For heterooctahedral micas an approach was adopted according to which M3 is always the larger cis cation. Although the group of heterooctahedral micas would benefit from more data, the equations (Tables 4, 5) afford realistic estimates of octahedral geometry for detected (e.g., Mössbauer) or anticipated ordering schemes and allow the user to fathom octahedral distortions before the results of a structural refinement are available. Possible ordering in micas other than homooctahedral, which must be decided upon before the equations in Tables 4, 5 are applied, can be devised

according to the distribution of individual elements between larger and smaller octahedra (Table 3). Better predictions should make better results easier to obtain, improving thus our understanding of the structural details in this important mineral group.

In conclusion let us observe that although plots with impressive correlations have been obtained, in some there is more scatter than one would expect. Of course, scatter may be a liability of the site-size approach in which charges are ignored. Also, the definitions of all functions representing distortions embody some oversimplification. Unable to fully express the complexity of individual polyhedra, these functions must introduce some scatter. Another possible cause may be the practice of refining structures in supergroup rather than subgroup symmetries (see Guggenheim and Bailey, 1977). As a consequence, possible octahedral orderings in some micas may have been suppressed or overlooked and the distortion functions may have become somewhat unrealistic. No correction short of a new refinement is possible here, but future projects should benefit from the hindsight and, hopefully, yield data with less bias.

Table 5. Constants in regression equations for predicting counter-rotation δ from mean bond lengths $\bar{d}$(M-A)$_{obs}$ and ^{1}MEFIR$_{obs}$.*

Equation for		Micas (n) **			
		Heterooctahedral (7) ***		Mesooctahedral (39)	
		Regression based on		Regression based on	
		^{1}MEFIR$_{obs}$	$\bar{d}$(M-A)$_{obs}$	^{1}MEFIR$_{obs}$	$\bar{d}$(M-A)$_{obs}$
δ(M1)	a_1	-16.5	-1.3	δ(M1) = 0°	
	a_2	-129.6	-41.2	due to symmetry	
	a_3	25.4	40.9		
	a_4	87.4	3.3		
	r	0.956	0.9997		
δ(M2)	a_1	-122.0	41.5	56.5	58.8
	a_2	-449.7	24.1	-35.5	-32.9
	a_3	-182.2	-30.4	****	****
	a_4	560.6	-66.8	-17.0	-53.2
	r	0.928	0.900	0.931	0.949
δ(M3)	a_1	1.4	49.4		
	a_2	-251.8	-42.3		
	a_3	-48.6	-8.5	****	
	a_4	217.0	2.9		
	r	0.997	0.999		

* δ(M1,M2,M3) = a_1 ^{1}MEFIR$_{obs}$(M1) + a_2 ^{1}MEFIR$_{obs}$(M2) + a_3 ^{1}MEFIR$_{obs}$(M3) + a_4

δ(M1,M2,M3) = a_1 $\bar{d}$(M1-A)$_{obs}$ + a_2 $\bar{d}$(M2-A)$_{obs}$ + a_3 $\bar{d}$(M3-A)$_{obs}$ + a_4

** Homooctahedral micas are not included because their M2 is geometrically identical with M1, hence δ(M1) = δ(M2) = 0°.

*** Some of the errors (not shown) exceed the associated constants, apparently due to paucity of data.

**** M3 is not defined in mesooctahedral micas.

Acknowledgments

References

Appelo, C. A. J. (1978) Layer deformation and crystal energy of micas and related minerals. I. Structural models for 1M and 2M$_1$ polytypes. American Mineralogist, 63, 782–792.

Backhaus, K. O. (1983) Structure refinement of an [sic] 1M-lepidolite. Crystal Research and Technology, 18, 1253–1260.

Barry, T. L. and Roy, Rustum (1967) Effective radius of a vacancy, and the calculation of solubility limits in crystals of highly ionic phases of the NaCl structure type. Zeitschrift für Kristallographie, 125, 70–79.

Birle, J. D. and Tettenhorst, Rodney (1968) Refined muscovite structure. Mineralogical Magazine, 36, 883–886.

Brown, B. E. (1978) The crystal structure of a 3T lepidolite. American Mineralogist, 63, 332–336.

Donnay, Gabrielle, Donnay, J. D. H., and Takeda, Hiroshi (1964) Trioctahedral one-layer micas. II. Prediction of the structure from composition and cell dimensions. Acta Crystallographica, 17, 1374–1381.

Donnay, Gabrielle, Morimoto, N., Takeda, Hiroshi, and Donnay, J. D. H. (1964) Trioctahedral one-layer micas. I. Crystal structure of a synthetic iron mica. Acta Crystallographica, 17, 1369–1373.

Drits, V. A. (1975) Structural and crystallochemical peculiarities of layer silicates. (in Russian) In Kristallokhimiya mineralov i geologicheskie problemy, p. 35–51. Nauka, Moskva.

Guggenheim, Stephen (1981) Cation ordering in lepidolite. American Mineralogist, 66, 1221–1232.

Guggenheim, Stephen and Bailey, S. W. (1975) Refinement of the margarite structure in subgroup symmetry. American Mineralogist, 60, 1023–1029.

Guggenheim, Stephen and Bailey, S. W. (1977) The refinement of zinnwaldite-1M in subgroup symmetry. American Mineralogist, 62, 1158–1167.

Güven, Necip (1971) The crystal structure of 2M$_1$ phengite and 2M$_1$ muscovite. Zeitschrift für Kristallographie, 134, 196–212.

Güven, Necip and Burnham, C. W. (1967) The crystal structure of 3T muscovite. Zeitschrift für Kristallographie, 125, 163–183.

Hazen, R. M. and Burnham, C. W. (1973) The crystal structures of one-layer phlogopite and annite. American Mineralogist, 58, 889–900.

Hazen, R. M. and Wones, D. R. (1972) The effect of cation substitutions on the physical properties of trioctahedral micas. American Mineralogist, 57, 103–129.

Hazen, R. M., Finger, L. W., and Velde, D. (1981) Crystal struc-

ture of a silica- and alkali-rich trioctahedral mica. American Mineralogist, 66, 586–591.

Hoppe, Rudolf (1979) Effective coordination numbers (ECoN) and mean fictive ionic radii (MEFIR). Zeitschrift für Kristallographie, 150, 23–52.

Joswig, W. (1972) Neutronenbeugungsmessungen an einem 1M-Phlogopit. Neues Jahrbuch für Mineralogie, Monatshefte, 1–11.

Kato, Toshio, Miura, Yasunori, Yoshii, Morimasa, and Maeda, Kenjiro (1979) The crystal structures of 1M-kinoshitalite, a new barium brittle mica and 1M-manganese trioctahedral micas. Mineralogical Journal, 9, 392–408.

Lin, Cheng-yi and Bailey, S. W. (1984) The crystal structure of paragonite-2M_1. American Mineralogist, 69, 122–127.

Lin, Jiunn-Chorng and Guggenheim, Stephen (1983) The crystal structure of a Li,Be-rich brittle mica: a dioctahedral–trioctahedral intermediate. American Mineralogist, 68, 130–142.

McCauley, J. W. and Newnham, R. E. (1973) Structure refinement of a barium mica. Zeitschrift für Kristallographie, 137, 360–367.

McCauley, J. W., Newnham, R. E., and Gibbs, G. V. (1973) Crystal structure analysis of synthetic fluorophlogopite. American Mineralogist, 58, 249–254.

Ohta, Tsutomu, Takeda, Hiroshi, and Takéuchi, Yoshio (1982) Mica polytypism: similarities in the crystal structures of coexisting 1M and 2M_1 oxybiotite. American Mineralogist, 67, 298–310.

Pavlishin, V. I., Semenova, T. F., and Rozhdestvenskaya, I. V. (1981) Protolithionite-3T: its structure, typomorphism, and practical significance. (in Russian) Mineralogicheskii zhurnal, 3, 1, 47–60.

Radoslovich, E. W. (1960) The structure of muscovite, KAl_2 $(Si_3Al)O_{10}(OH)_2$. Acta Crystallographica, 13, 919–932.

Radoslovich, E. W. and Norrish, K. (1962) The cell dimensions and symmetry of layer-lattice silicates I. Some structural considerations. American Mineralogist, 47, 599–616.

Rayner, J. H. (1974) The crystal structure of phlogopite by neutron diffraction. Mineralogical Magazine, 39, 850–856.

Richardson, S. M. and Richardson, J. W., Jr. (1982) Crystal structure of a pink muscovite from Archer's Post, Kenya: implications for reverse pleochroism in dioctahedral micas. American Mineralogist, 67, 69–75.

Robert, J.-L. and Gasperin, M. (1984) Crystal structure refinement of hendricksite, a Zn- and Mn- rich trioctahedral potassium mica; a contribution to the crystal chemistry of zinc-bearing minerals. Tschermaks Mineralogische und Petrographische Mitteilungen, in press.

Rothbauer, R. (1971) Untersuchung eines 2M_1-Muskovits mit Neutronenstrahlen. Neues Jahrbuch für Mineralogie, Monatshefte, 143–154.

Rozhdestvenskaya, I. V. and Frank-Kamenetskii, V. A. (1974) Structure of the dioctahedral mica chernykhite. (in Russian) In V. A. Frank-Kamenetskii et al., Eds., Kristallokhimiya i struktura mineralov, p. 28–33. Nauka, Leningrad.

Sartori, F. (1976) The crystal structure of a 1M lepidolite. Tschermaks Mineralogische und Petrographische Mitteilungen, 23, 65–75.

Sartori, F. (1977) The crystal structure of a 2M_1 lepidolite. Tschermaks Mineralogische und Petrographische Mitteilungen, 24, 23–37.

Sartori, Franco, Franzini, Marco, and Merlino, Stefano (1973) Crystal structure of a 2M_2 lepidolite. Acta Crystallographica, B29, 573–578.

Semenova, T. F., Rozhdestvenskaya, I. V., and Frank-Kamenetskii, V. A. (1977) Refinement of the crystal structure of

tetraferriphlogopite. (in Russian) Kristallografiya, 22, 1196–1201.

Shannon, R. D. (1976) Revised effective ionic radii and systematic studies of interatomic distances in halides and chalcogenides. Acta Crystallographica, A32, 751–767.

Sidorenko, O. V., Zvyagin, B. B., and Soboleva, S. V. (1975) Refinement of the crystal structure of a 1M dioctahedral mica. (in Russian) Kristallografiya, 20, 543–549.

Sidorenko, O. V., Zvyagin, B. B., and Soboleva, S. V. (1977) Refinement of the crystal structure of paragonite 2M_1 by high-voltage electron diffraction. (in Russian) Kristallografiya, 22, 971–975.

Sidorenko, O. V., Zvyagin, B. B., and Soboleva, S. V. (1977) Crystal structure of paragonite 3T. (in Russian) Kristallografiya, 22, 976–981.

Soboleva, S. V. and Zvyagin, B. B. (1968) Crystal structure of a 1M dioctahedral Al-mica. (in Russian) Kristallografiya, 13, 605–610.

Soboleva, S. V., Sidorenko, O. V., and Zvyagin, B. B. (1977) Crystal structure of paragonite 1M. (in Russian) Kristallografiya, 22, 510–514.

Sokolova, G. V., Aleksandrova, V. A., Drits, V. A., and Bairakov, V. V. (1979) Crystal structures of two lithium-bearing brittle micas. (in Russian) In V. A. Frank-Kamenetskii, Ed., Kristallokhimiya i strukturnaya mineralogiya, p. 55–66. Nauka, Leningrad.

Steinfink, Hugo (1962) Crystal structure of a trioctahedral mica: phlogopite. American Mineralogist, 47, 886–896.

Swanson, T. H. and Bailey, S. W. (1981) Redetermination of the lepidolite 2M_1 structure. Clays and Clay Minerals, 29, 81–90.

Takeda, Hiroshi and Burnham, C. W. (1969) Fluor-polylithionite: a lithium mica with nearly hexagonal $(Si_2O_5)^{2-}$ ring. Mineralogical Journal, 6, 102–109.

Takeda, Hiroshi and Donnay, J. D. H. (1966) Trioctahedral one-layer micas. III. Crystal structure of a synthetic lithium fluormica. Acta Crystallographica, 20, 638–646.

Takeda, Hiroshi and Ross, Malcolm (1975) Mica polytypism: dissimilarities in the crystal structures of coexisting 1M and 2M_1 biotite. American Mineralogist, 60, 1030–1040.

Takeda, Hiroshi, Haga, N., and Sadanaga, R. (1971) Structural investigation of polymorphic transitions between 2M_2-, 1M-lepidolite and 2M_1 muscovite. Mineralogical Journal, 6, 203–215.

Takéuchi, Y. (1965) Structures of brittle micas. Proceedings of the 13th National Conference 1964, Madison, 1–25, Pergamon Press, Oxford.

Tateyama, Hiroshi, Shimoda, Susumo, and Sudo, Toshio (1974) The crystal structure of synthetic Mg^{IV} mica. Zeitschrift für Kristallographie, 139, 196–206.

Toraya, Hideo (1981) Distortions of octahedra and octahedral sheets in 1M micas and the relation to their stability. Zeitschrift für Kristallographie, 157, 173–190.

Toraya, Hideo and Marumo, Fumiyuki (1983) The crystal structure of a germanate mica $KMg_{2.5+x}Ge_{4-2x}Al_{2x}O_{10}F_2$ ($x \approx 0.14$) and distortion of (Ge,Al)O_4 tetrahedra. Mineralogical Journal, 11, 222–231.

Toraya, Hideo, Marumo, Fumiyuki, and Hiráo, Minoru (1983) Synthesis and the crystal structure of a manganoan fluoromica, $K(Mg_{2.44}Mn_{0.24})(Si_{3.82}Mg_{0.18})O_{10}F_2$. Mineralogical Journal, 11, 240–247.

Toraya, H., Iwai, S., Marumo, F., and Hirao, M. (1977) The crystal structure of taeniolite, $KLiMg_2Si_4O_{10}F_2$. Zeitschrift für Kristallographie, 146, 73–83.

Toraya, H., Iwai, S., Marumo, F., and Hirao, M. (1978) The crystal structures of germanate micas, $KMg_{2.5}Ge_4O_{10}F_2$ and $KLiMg_2Ge_4O_{10}F_2$. Zeitschrift für Kristallographie, 148, 65–81.

Toraya, Hideo, Iwai, Shin-ichi, Marumo, Fumiyuki, and Hirao, Minoru (1978) The crystal structure of a germanate mica, $KMg_3Ge_3AlO_{10}F_2$. Mineralogical Journal, 9, 221–230.

Toraya, H., Iwai, S., Marumo, F., Daimon, M., and Kondo, R. (1976) The crystal structure of tetrasilicic potassium fluor mica, $KMg_{2.5}Si_4O_{10}F_2$. Zeitschrift für Kristallographie, 144, 42–52.

Toraya, Hideo, Iwai, Shin-ichi, Marumo, Fumiyuki, Nishikawa, Tadahiro, Hirao, Minoru (1978) The crystal structure of synthetic mica, $KMg_{2.75}Si_{3.5}Al_{0.5}O_{10}F_2$. Mineralogical Journal, 9, 210–220.

Tsipurskii, S. I. and Drits, V. A. (1977) The effectivity of electronometric measurement of intensities in structural investigation by electron diffraction. (in Russian) Izvestiya Akademii nauk SSSR, Seriya fizicheskaya, 41, 2263–2271.

Zhoukhlistov, A. P., Zvyagin, B. B., Soboleva, S. V., and Fedotov, A. F. (1973) The crystal structure of the dioctahedral mica $2M_2$ determined by high voltage electron diffraction. Clays and Clay Minerals, 21, 465–470.

Zhukhlistov, A. P., Zvyagin, B. B., Lazarenko, E. K., and Pavlishin, V. I. (1977) Refinement of the crystal structure of a ferruginous celadonite. (in Russian) Kristallografiya, 22, 498–504.